

Probing Quantum Capacitance in a 3D Topological Insulator

D. A. Kozlov,^{1,2,3} D. Bauer,³ J. Ziegler,³ R. Fischer,³ M. L. Savchenko,^{1,2} Z. D. Kvon,^{1,2}
N. N. Mikhailov,¹ S. A. Dvoretzky,¹ and D. Weiss³

¹*A. V. Rzhanov Institute of Semiconductor Physics, Novosibirsk 630090, Russia*

²*Novosibirsk State University, Novosibirsk 630090, Russia*

³*Experimental and Applied Physics, University of Regensburg, D-93040 Regensburg, Germany*

(Received 3 November 2015; revised manuscript received 7 December 2015; published 22 April 2016)

We measure the quantum capacitance and probe thus directly the electronic density of states of the high mobility, Dirac type two-dimensional electron system, which forms on the surface of strained HgTe. Here we show that observed magnetocapacitance oscillations probe—in contrast to magnetotransport—primarily the top surface. Capacitance measurements constitute thus a powerful tool to probe only one topological surface and to reconstruct its Landau level spectrum for different positions of the Fermi energy.

DOI: 10.1103/PhysRevLett.116.166802

Three-dimensional topological insulators (3D TI) represent a new class of materials with insulating bulk and conducting two-dimensional surface states [1–4]. The properties of these surface states are of particular interest as they have a spin degenerate, linear Dirac-like dispersion with spins locked to their electrons' k vectors [4,5]. Strained HgTe, examined here, constitutes a 3D TI with high electron mobilities allowing the observation of Landau quantization and quantum Hall steps down to low magnetic fields [6,7]. While unstrained HgTe is a zero gap semiconductor with inverted band structure [8,9], the degenerate Γ_8 states split and a gap opens at the Fermi energy E_F if strained. This system is a strong topological insulator [10], explored by transport [6,7,11], angle-resolved photoemission spectroscopy [12], photoconductivity, and magneto-optical experiments [13–16]; also, the proximity effect has been investigated [17]. Since these two-dimensional electron states (2DES) have high electron mobilities of several 10^5 cm²/Vs, pronounced Shubnikov–de Haas (SdH) oscillations of the resistivity and quantized Hall plateaus commence in quantizing magnetic fields [6,7,11], stemming from both top and bottom 2DES. The oscillations stem from Landau quantization which strongly modifies the density of states (DOS). Capacitance spectroscopy allows us to directly probe the thermodynamic DOS $dn/d\mu$ (n = carrier density, μ = electrochemical potential), denoted as D , of a 3D TI. The total capacitance measured between a metallic top gate and a 2DES depends, besides the geometric capacitance, on the quantum capacitance e^2D , connected in series and reflecting the finite density of states D of the 2DES [18–22]; e is the elementary charge. Below, the quantum capacitance of the top surface is denoted as e^2D_t , the one of the bottom layer by e^2D_b . We show that capacitance measures, in contrast to transport, the properties of a single Dirac cone in a 3D TI.

The experiments are carried out on strained 80 nm thick HgTe films, grown by molecular beam epitaxy on

CdTe (013). For details, see [16]. The Dirac surface electrons have high electron mobilities of order 4×10^5 cm²/Vs. The cross section of the structure is sketched in Fig. 1(a). For transport and capacitance measurements, carried out on one and the same device, the films were patterned into Hall bars with metallic top gates. Several devices from the same wafer have been studied. The measurements were performed at temperature $T = 1.5$ K and in magnetic fields B up to 13 T. For magnetotransport measurements the standard lock-in technique has been applied. For the capacitance measurements we superimpose the dc bias V_g with a small ac voltage and measure the ac current flowing across our device phase sensitively. The absence of both leakage currents and

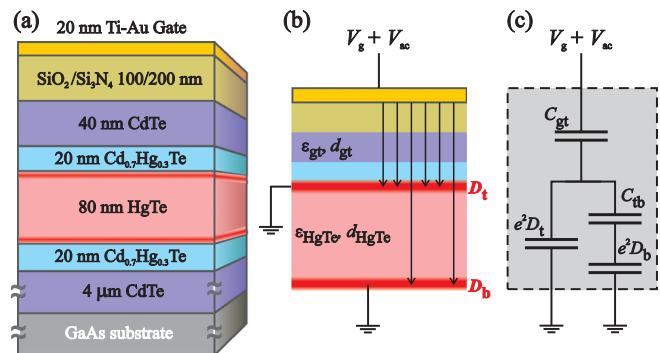


FIG. 1. (a) Cross section of the heterostructures studied. The Dirac surface states (red) enclose the strained HgTe layer. (b) Schematics of the “three plate capacitor” formed by the metallic top gate and top and bottom layer (red) with density of states D_t and D_b , respectively. The electric field (black arrows) is partially screened by the top surface layer. (c) Corresponding equivalent circuit with the quantum capacitances Ae^2D_t and Ae^2D_b in series with the respective geometrical capacitances. The equivalent circuit is the one introduced in [22], but extended by the quantum capacitance of the bottom surface, Ae^2D_b . A similar equivalent circuit was recently introduced in [23].

resistive effects were controlled by the real part of the measured ac current.

When the Fermi level (electrochemical potential) is located in the bulk gap the system can be viewed as a “three-plate” capacitor where the top and bottom surfaces form the two lower plates [see Fig. 1(b) and the corresponding equivalent circuit in Fig. 1(c)]. From this equivalent circuit it follows that, as long as D_b does not vanish, the measured total capacitance is more sensitive to changes of D_t than of D_b ; the explicit connection between D_t , D_b and total capacitance C is given in the Supplemental Material [24]. The ratio of $(dC/dD_t)/(dC/dD_b) = (AD_b e^2 + C_{\text{tb}})^2 / C_{\text{tb}}^2$ is significantly larger than unity since $AD_b e^2 + C_{\text{tb}}$ is (at $B = 0$) at least a factor of 2 larger than C_{tb} . Here, C_{tb} is the geometric capacitance $C_{\text{tb}} = \epsilon_{\text{HgTe}} \epsilon_0 A / d_{\text{HgTe}}$ between top and bottom surface, with $\epsilon_{\text{HgTe}} \approx 21$, the dielectric constant of HgTe [25], d_{HgTe} is the thickness of the HgTe film, A is the gated TI area, and ϵ_0 the dielectric constant of vacuum. Therefore, the measured capacitance reflects primarily the top surface’s DOS, D_t . In the limit $C_{\text{tb}} \rightarrow 0$ or $e^2 D_b \rightarrow 0$ the total capacitance C is given by the expression usually used for conventional 2DES: $1/C = 1/C_{\text{gt}} + 1/Ae^2 D$ with the geometric capacitance $C_{\text{gt}} = \epsilon_{\text{gt}} \epsilon_0 A / d_{\text{gt}}$, where ϵ_{gt} is the dielectric constant of the layers between gate and top 2DES, d_{gt} is the corresponding thickness [20,21]. Note that $C_{\text{gt}} \ll e^2 D_t$; therefore, variations of the DOS cause only small changes of C . First quantum capacitance measurements have been reported for Bi₂Se₃, but the experiments were carried out at high frequencies at which resistive effects prevail [26].

Typical ρ_{xx} and ρ_{xy} traces as function of V_g are shown in Fig. 2(a). ρ_{xx} displays a maximum near $V_g = 1.5$ V, whereas ρ_{xy} changes sign; this occurs in the immediate vicinity of the charge neutrality point (CNP) [7]. The corresponding capacitance $C(V_g)$ at $B = 0$ in Fig. 2(b) exhibits a broad minimum between 2.2 and 4.5 V and echoes the reduced DOS D_t and D_b of the Dirac 2DES when the Fermi energy E_F is in the gap of HgTe. For $V_g > 4.5$ V, E_F moves into the conduction band where surface electrons coexist with the bulk ones. There, the capacitance (and thus the DOS) is increased and grows only weakly with increasing V_g . The weak increase of C with $|V_g|$, is ascribed to an increase of C_{gt} at higher $|V_g|$ since the carriers’ wave function is “pressed” towards the interface, an effect neglected in our description [20,21]. Reducing V_g below 2.2 V shifts E_F below the valence band edge so that surface electrons and bulk holes coexist. A strong positive magnetoresistance, a nonlinear Hall voltage, and a strong temperature dependence of ρ_{xx} provide independent confirmation that E_F is in the valence band [7]. Because of the valley degeneracy of holes in HgTe and the higher effective mass, the DOS, and therefore the measured capacitance C is highest in the valence band.

For B well below 1 T both $C(V_g)$ and $\rho_{xx}(V_g)$ start to oscillate and herald the formation of Landau levels (LLs).

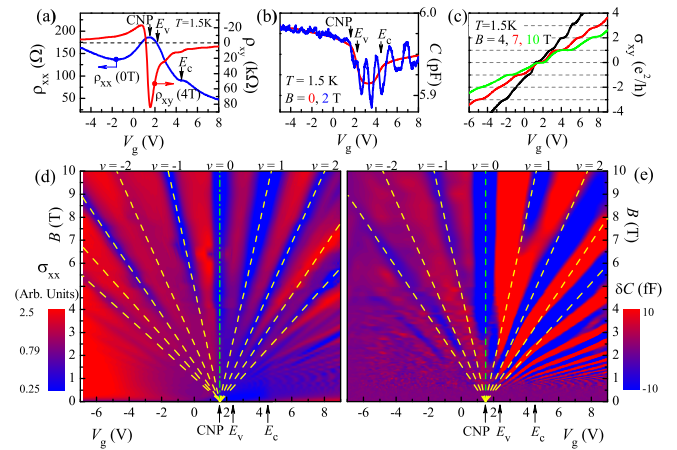


FIG. 2. (a) Typical $\rho_{xx}(V_g)$ and $\rho_{xy}(V_g)$ traces measured at $B = 0$ and $B = 4$ T. ρ_{xx} displays a maximum and ρ_{xy} changes sign around the CNP. (b) Capacitance measured at $B = 0$ and $B = 2$ T. The pronounced minimum of the $B = 0$ capacitance corresponds to the reduced DOS when E_F is in the gap. Hence, the band edges are at $E_v \approx 2.2$ V and $E_c \approx 4.4$ V. The quantum oscillations of the capacitance reflect the oscillations of the DOS. (c) Hall conductivity $\sigma_{xy}(V_g)$ measured for $B = 4$ T (black), 7 T (red), and 10 T (green). Quantized steps occur on the hole and electron side. (d) 2D color map of normalized $\sigma_{xx}(V_g, B)$ data. The red color stands for σ_{xx} maxima while the blue color displays minima. From the distance between the σ_{xx} minima we extract a filling rate of $\alpha_{\text{total}} = 7.6 \times 10^{10} \text{ cm}^{-2}/\text{V}$ (see text). This allows constructing a LL fan chart (dashed yellow lines) which describes the low filling factors ν well. (e) 2D color map of $\delta C(B) = C(B) - C(0)$ as function of B and V_g . As in (d), the blue color displays gaps between LLs (DOS minima). The LL fan chart is the same as in (d). CNP, E_c , and E_v are marked on the x axis.

The $C(V_g)$ trace oscillates around the $B = 0$ capacitance, shown for $B = 2$ T in Fig. 2(b). These oscillations, reflecting DOS oscillations, are more pronounced on the electron side (right of the CNP). This electron-hole asymmetry stems mainly from the larger hole mass, leading to reduced LL separation for the holes. At higher fields Hall conductivity σ_{xy} and resistivity ρ_{xy} (not shown) become fully quantized. $\sigma_{xy}(V_g)$, shown for $B = 4, 7$, and 10 T in Fig. 2(c), shows quantized steps of height e^2/h ($h = \text{Planck's constant}$), as expected for spin-polarized 2DES.

Transport and capacitance data in the whole V_g and B space are presented in Figs. 2(d) and 2(e) as 2D color maps (see Supplemental Material [24] for additional information). We start with discussing $\sigma_{xx} = \rho_{xx}/(\rho_{xx}^2 + \rho_{xy}^2)$ data in Fig. 2(d) first. The sequence of σ_{xx} extrema is almost symmetrical to the CNP where electron and hole densities match. At fixed B the distance ΔV_g between neighboring σ_{xx} minima corresponds to a change of density $\Delta n = eB/h$ from which we calculate the filling rate $dn/dV_g = \alpha_{\text{total}} = 7.6 \times 10^{10} \text{ cm}^{-2}/\text{V}$ at 10 T. The filling rate α_{total} describes the change of the total carrier density n with V_g . Comparison of electron densities extracted in the classical Drude regime with densities taken from the periodicity of

SdH oscillations have shown that σ_{xx} oscillations at high B reflect the total carrier density in the TI, i.e., charge carrier densities in the bulk plus in top and bottom surfaces [7]. α_{total} is directly proportional to $C/A = e\alpha_{\text{total}}/dV_g$ and corresponds to $C/A = e\alpha_{\text{total}} = 1.22 \times 10^{-4} \text{ F/m}^2$, a value close to the calculated capacitance $C_{\text{gt}}^{\text{calc}}/A = 1.45 \times 10^{-4} \text{ F/m}^2$ using thickness and dielectric constant of the layers [see Figs. 1(a) and 1(c) and the Supplemental Material [24]]. Using this α_{total} , the Landau level fan, i.e., the calculated positions of the σ_{xx} minima as a function of V_g and B , fits the data for low filling factors ν quite well. For ν larger than 2 on the electron side the fan chart significantly deviates from experiment and is discussed using higher resolution data below. On the hole side where SdH oscillations stem from bulk holes, fan chart and experimental data match almost over the whole (V_g, B) range. We now turn to the magnetocapacitance data $\delta C = C(V_g, B) - C(V_g, B = 0)$ shown in Fig. 2(e). The data are compared to the same fan chart derived from transport. On the electron side, measured δC minima display a reduced slope compared to the transport fan chart, pointing to a reduced filling rate. This is a first indication that capacitance does not reflect the total carrier density in the system but predominantly the one of the top 2DES only. On the hole side the LL fan chart fits the data quite well but in contrast to transport, LL features are less well resolved there. This asymmetry is related with the different effective masses; the enhanced visibility in transport is due to that fact that SdH oscillations depend on D^2 while the capacitance depends on D only.

Previous transport experiments have shown that the periodicity of the SdH oscillations is changed at small B , corresponding to a reduced carrier density [7]. While at high fields the SdH oscillations reflect the total carrier density they echo the carrier density of the top surface at sufficiently low B . This is due to the fact that SdH oscillations get, with increasing B , first resolved in the layer with the higher density and mobility, i.e., higher partial conductivity and lower LL level broadening [7].

We now compare data taken at B up to 4 T, displayed in Figs. 3(a) and 3(b), which show marked differences between transport and capacitance. We start with discussing the capacitance data first. The capacitance [Fig. 3(b)] shows uniform oscillations of δC with maxima positions, corresponding to different LLs, which are perfectly fitted by two fan charts featuring a distinct crossover at about $V_g = 4.4 \text{ V}$. The crossover stems from E_F entering the conduction band causing a reduced filling rate for $V_g > 4.4 \text{ V}$. From the distance of δC minima (or maxima) at constant B we can extract the filling rate $\alpha_{\text{top}}^{\text{gap}}$ in the gap ($2.2 \text{ V} < V_g < 4.4 \text{ V}$) and for E_F in the conduction band, $\alpha_{\text{top}}^{\text{bulk}}$. From Fig. 3(b) we obtain $\alpha_{\text{top}}^{\text{gap}} = 5.25 \times 10^{10} \text{ cm}^{-2}/\text{V}$ and $\alpha_{\text{top}}^{\text{bulk}} = 3.3 \times 10^{10} \text{ cm}^{-2}/\text{V}$. This means that in the gap $\alpha_{\text{top}}^{\text{gap}}/\alpha_{\text{total}} = 70\%$ of the total filling rate apply to the top surface while the remaining 30% can be

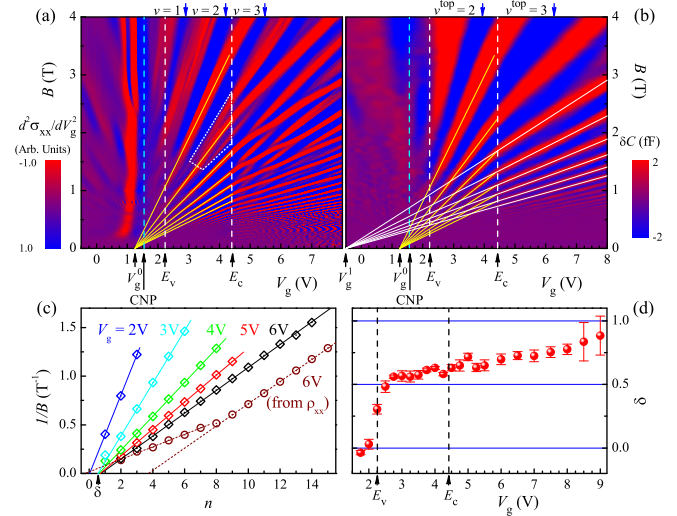


FIG. 3. (a) 2D color map of $d^2\sigma_{xx}/dV_g^2$ between 0 and 4 T. The red color indicates σ_{xx} maxima, the blue color LL's gaps. The yellow fan chart, here marking in contrast to Fig. 2 LLs, is the one taken from (b). Already in the gap the LLs branch out, marked by the dotted window and for $V_g > 4.5 \text{ V}$ the data can no longer be described by a simple fan; the pattern is entangled in a complicated way, suggesting that electrons of top and bottom surface and the bulk contribute. (b) Capacitance data corresponding to (a) show a quite regular Landau fan chart. The experimental data can be fitted by two fan charts originating at V_g^0 and V_g^1 . The different slope of the two fan charts resembles the different filling rates $\alpha_{\text{top}}^{\text{gap}}$ and $\alpha_{\text{top}}^{\text{bulk}}$ (see text). (c) δC minima for $V_g = 2, \dots, 6 \text{ V}$ and ρ_{xx} minima for $V_g = 6 \text{ V}$ positions on a $1/B$ scale. (d) Phase of the δC oscillations as a function of V_g . The gap is marked by vertical dashed lines.

ascribed to the bottom surface. The reduced $\alpha_{\text{top}}^{\text{bulk}}$ for E_F in the conduction band is $0.44\alpha_{\text{total}}$ and hence the remaining filling rate of 56% is shared between bulk and back surface filling. We note that we obtain reasonable values for the filling rates only when we assume spin-resolved LLs. Since there is no signature of spin splitting down to 0.6 T, where the oscillations fade, the quantum oscillations stem from nondegenerate LLs, proving the topological nature of the charge carriers. The extrapolation of the two fan charts towards $B \rightarrow 0$ defines two points on the V_g axis, denoted as $V_g^0 = 1.25 \text{ V}$ and $V_g^1 = -0.5 \text{ V}$. These points correspond to vanishing electron density n_{top} on the top surface in case the respective filling rates $\alpha_{\text{top}}^{\text{gap}}$ and $\alpha_{\text{top}}^{\text{bulk}}$ would stay constant over the entire V_g range. This is not the case as $\alpha_{\text{top}}^{\text{bulk}} = \text{constant}$ only applies for E_F in the conduction band and $\alpha_{\text{top}}^{\text{gap}} = \text{constant}$ for E_F in the gap. Moving E_F into the valence band greatly reduces this filling rate. Therefore, V_g^0 and V_g^1 correspond only to virtual zeros of the electron density while the real one is much deeper in the valence band.

We now turn to the transport data in Fig. 3(a). To get a better resolution of the low field SdH oscillations we plot $d^2\sigma_{xx}/dV_g^2$ in Fig. 3(a); as before, red regions indicate σ_{xx}

maxima. While the same LL fan fits the low B -field data (a close-up of the data is shown and discussed in the Supplemental Material [24]) striking deviations occur at higher B . (i) Transport data for E_F in the gap show splitting of the LLs and for $V_g > 4.4$ V; i.e., for E_F in the conduction band, a very complex structure with crossing LLs evolves. (ii) The filling factors given on top of Fig. 3(b) are the ones of the electrons in the top surface only, while the filling factors given in Fig. 3(a) are the ones of the total carrier density. (iii) Extra splitting of the maxima occurs also in the gap region, most pronounced in the marked region. We thus conclude that in transport the three available transport channels (top, bottom surface electrons, bulk electrons) contribute to the signal and lead to a complicated pattern of the quantum oscillations as a function of B and V_g , involving transport via side facets. The oscillations of δC , in contrast, stem preferentially from the top surface and allow probing the LL spectrum of a single Dirac surface. Corrections to that likely occur at high B and V_g ; a level splitting at ($V_g \approx 7$ V, $B \approx 3$ T) in Fig. 3(b) suggests that signals from bulk or back surface can affect also δC at higher B , although to a far lesser degree when compared to transport.

The fact that the data are best described by spin-resolved LL degeneracy indicates the surface states' topological nature. The phase of the quantum oscillations δ defined by $(1/B_{\min,n})/\Delta_{1/B} = n + \delta$ is another indicator of topological surface states [27]. Here, $B_{\min,n}$ is the magnetic field position of the n th oscillation minimum and $\Delta_{1/B}$ is the period of the oscillations on the $1/B$ scale. The phase can be obtained by plotting the integer oscillation index n vs $1/B_{\min,n}$. This is shown in Fig. 3(c) both for δC ($V_g = 2, \dots, 6$ V) and transport oscillations (for $V_g = 6$ V). While the δC minima lie on straight lines with intercepts δ shown in Fig. 3(d), the corresponding transport minima display two slopes. At low fields, where the oscillations stem from the top surface only, the phase factor is $\delta = 0.72 \pm 0.04$ showing the same value as extracted from capacitance = 0.7 ± 0.04 , but for high field SdH oscillations, stemming from both layers, $\delta \sim 0$, as for conventional 2DES. In Fig. 3(d) we show the evolution of δ as a function of V_g . For E_F in the gap δ is close to 0.5 expected for ideal Dirac fermions of a single surface. δ vanishes quickly for E_F entering the valence band and gradually for increasing V_g . The latter we ascribe to increasing hybridization of the surface and bulk states deep in the conduction band. Our experiments prove that a finite phase δ which is a direct fingerprint of the Berry phase acquired by electrons in B fields, can only be observed if the oscillations stem from a single topological surface.

In summary, we present measurements of the quantum capacitance of a TI which directly reflects the DOS of Dirac surface states. The magneto-oscillations of the quantum capacitance allow tracing the LL structure of a single Dirac

surface. The complimentary information provided by transport and capacitance experiments is promising in getting a better understanding of the electronic structure of TIs, the latter being particularly important for potential applications of this new class of materials.

We acknowledge funding by the Elite Network of Bavaria (K-NW-2013-258), by the German Science Foundation (DFG) via SPP 1666 and by the Volkswagen Foundation. This work was partially supported by RFBR Grants No. 14-02-31631, No. 15-32-20828, and No. 15-52-16008.

-
- [1] M. Z. Hasan and C. L. Kane, *Rev. Mod. Phys.* **82**, 3045 (2010).
 - [2] J. E. Moore, *Nature (London)* **464**, 194 (2010).
 - [3] X.-L. Qi and S.-C. Zhang, *Rev. Mod. Phys.* **83**, 1057 (2011).
 - [4] Y. Ando, *J. Phys. Soc. Jpn.* **82**, 102001 (2013).
 - [5] C. L. Kane and E. J. Mele, *Phys. Rev. Lett.* **95**, 226801 (2005).
 - [6] C. Brune, C. X. Liu, E. G. Novik, E. M. Hankiewicz, H. Buhmann, Y. L. Chen, X. L. Qi, Z. X. Shen, S. C. Zhang, and L. W. Molenkamp, *Phys. Rev. Lett.* **106**, 126803 (2011).
 - [7] D. A. Kozlov, Z. D. Kvon, E. B. Olshanetsky, N. N. Mikhailov, S. A. Dvoretzky, and D. Weiss, *Phys. Rev. Lett.* **112**, 196801 (2014).
 - [8] S. H. Groves, R. N. Brown, and C. R. Pidgeon, *Phys. Rev.* **161**, 779 (1967).
 - [9] K. Seeger, *Semiconductor Physics*, Springer Series in Solid State Sciences Vol. 40 (Springer, Berlin, 1985).
 - [10] L. Fu and C. L. Kane, *Phys. Rev. B* **76**, 045302 (2007).
 - [11] C. Brune, C. Thienel, M. Stuibler, J. Bottcher, H. Buhmann, E. G. Novik, C.-X. Liu, E. M. Hankiewicz, and L. W. Molenkamp, *Phys. Rev. X* **4**, 041045 (2014).
 - [12] O. Crauste, Y. Ohtsubo, P. Ballet, P. A. L. Delplace, D. Carpentier, C. Bouvier, T. Meunier, A. Taleb-Ibrahimi, and L. Levy, *arXiv:1307.2008* (2013).
 - [13] A. M. Shuvaev, G. V. Astakhov, C. Brune, H. Buhmann, L. W. Molenkamp, and A. Pimenov, *Semicond. Sci. Technol.* **27**, 124004 (2012).
 - [14] A. M. Shuvaev, G. V. Astakhov, M. Muhlbauer, C. Brune, H. Buhmann, and L. W. Molenkamp, *Appl. Phys. Lett.* **102**, 241902 (2013).
 - [15] A. M. Shuvaev, G. V. Astakhov, G. Tkachov, C. Brune, H. Buhmann, L. W. Molenkamp, and A. Pimenov, *Phys. Rev. B* **87**, 121104(R) (2013).
 - [16] K.-M. Dantscher, D. A. Kozlov, P. Olbrich, C. Zoth, P. Faltermeier, M. Lindner, G. V. Budkin, S. A. Tarasenko, V. V. Bel'kov, Z. D. Kvon, N. N. Mikhailov, S. A. Dvoretzky, D. Weiss, B. Jenichen, and S. D. Ganichev, *Phys. Rev. B* **92**, 165314 (2015).
 - [17] I. Sochnikov, L. Maier, C. A. Watson, J. R. Kirtley, C. Gould, G. Tkachov, E. M. Hankiewicz, C. Brune, H. Buhmann, L. W. Molenkamp, and K. A. Moler, *Phys. Rev. Lett.* **114**, 066801 (2015).
 - [18] F. Stern, *Appl. Phys. Lett.* **43**, 974 (1983).
 - [19] T. P. Smith, B. B. Goldberg, P. J. Stiles, and M. Heiblum, *Phys. Rev. B* **32**, 2696 (1985).

- [20] T. P. Smith, W. I. Wang, and P. J. Stiles, *Phys. Rev. B* **34**, 2995 (1986).
- [21] V. Mosser, D. Weiss, K. v Klitzing, K. Ploog, and G. Weimann, *Solid State Commun.* **58**, 5 (1986).
- [22] S. Luryi, *Appl. Phys. Lett.* **52**, 501 (1988).
- [23] Y. Baum, J. Bottcher, C. Brune, C. Thienel, L. W. Molenkamp, A. Stern, and E. M. Hankiewicz, *Phys. Rev. B* **89**, 245136 (2014).
- [24] See Supplemental Materials at <http://link.aps.org/supplemental/10.1103/PhysRevLett.116.166802> for details.
- [25] J. Baars and F. Sorger, *Solid State Commun.* **10**, 875 (1972).
- [26] F. Xiu, N. Meyer, X. Kou, L. He, M. Lang, Y. Wang, X. Yu, A. V. Fedorov, J. Zou, and K. L. Wang, *Sci. Rep.* **2**, 669 (2012).
- [27] A. A. Taskin and Y. Ando, *Phys. Rev. B* **84**, 035301 (2011).